



Bimetallic Structure of Ti6Al4V/IN718 with CuSi Interlayer for Wire-Arc Directed Energy Deposition Process

Avinash Mishra¹ · Amrit Raj Paul^{2,3} · Manidipto Mukherjee^{2,3} · Rabesh Kumar Singh⁴

Received: 16 October 2022 / Accepted: 28 December 2022 / Published online: 18 February 2023
© The Author(s) under exclusive licence to The Korean Institute of Metals and Materials 2023

Abstract

Fabricating bimetallic structures using various additive manufacturing processes is an ingenious way to integrate different material properties in a single component. This study offers a novel method for fabricating Ti6Al4V and IN718 bimetallic structures using a wire-arc-based directed energy deposition process with a CuSi interlayer, both with and without the addition of pure copper powder at the CuSi–Ti6Al4V interface. The Cu–Ti and Ni–Cu interfaces of the bimetallic structure have been examined in terms of their metallurgical and mechanical characteristics. The study revealed the presence of Cu₄Ti₃, Cu₃Ti₂, Cu₄Ti, CuTi₂ and Ti₅Si₃ phases at the Cu–Ti interface, whereas CuNi and NiCr₂ phases at the Ni–Cu interface. The Cu–Ti interface with copper powder shows two distinctive layers of intermetallic phases with less intermetallic thickness compared to the interface without copper powder. The maximum bonding strength of 152.31 ± 40.74 MPa and hardness of ~485 HV were achieved in the interface without a copper powder sample. However, for interface with copper powder sample, the presence of Ti₅Si₃ hindered the further transformation of less stable Cu–Ti phases resulting in decreased strength.

Keywords Bimetallic structures · Wire-arc directed energy deposition · Metallography · Intermetallic · Interface engineering

1 Introduction

Multi-material structures provide a competitive edge in fabricating highly functional components for demanding applications. Different properties of the material, such as thermo-physical, mechanical, electrical, and corrosion/oxidation resistance, might benefit the resulting multi-metallic structure. Metals can be directly bonded or compositionally graded to generate such multi-metallic structures. Direct bonding of various dissimilar metals has been challenging

for many years due to the sharp interface, which is vulnerable to cracking and delamination at locations with lower interfacial bonding due to the component materials' property mismatch. A metallurgical adhesive material interlayer, on the other hand, could be used to solve the problem by creating a diffusion barrier to avoid the development of a more undesired interface [1, 2]. Casting, explosive welding, diffusion bonding, powder metallurgy, and other traditional processes are used to fabricate bimetallic structures. However, due to intrinsic restrictions, these processes cannot be used to fabricate complex-shaped bimetallic components. Since the components can be printed layer by layer and the material composition in different layers can be easily altered, additive manufacturing (AM) technology is ideal for fabricating bimetallic structures. According to the ASTM F42 standard, the directed energy deposition (DED) technology, which encompasses a variety of terminologies such as laser-engineered net shaping (LENS) [3, 4], wire-arc directed energy deposition (WADED) [5, 6], and laser cladding [7], is ideal for producing such bimetallic and functionally graded structures (FGS).

WADED is a large-scale metal additive manufacturing (AM) technology that uses an arc as a heat source to fuse

✉ Manidipto Mukherjee
m.mukherjee.ju@gmail.com

✉ Rabesh Kumar Singh
rasm.singh@gmail.com

¹ Department of Mechanical Engineering, Indian Institute of Technology Tirupati, Tirupati 517506, India

² Central Mechanical Engineering Research Institute, Durgapur, West Bengal 713209, India

³ Academy of Scientific and Innovative Research, Ghaziabad, Uttar Pradesh 201002, India

⁴ Centre for Advanced Studies, Lucknow, Uttar Pradesh 226031, India

metallic wires for depositing material layer-by-layer to produce complicated shaped 3D components [8]. The benefits of WADED over other metal AM processes include cheap cost, high deposition rate, open architecture, high efficiency, etc., and it finds applications in the aerospace, automobile, and industries primarily because of the advantages discussed above [9]. Recent advancements in WADED technology have expanded the possibilities for fabricating bimetallic components. However, the deposition of different metals to produce such bimetallic structures utilising the WADED process may result in challenges such as the increased formation of brittle intermetallic at the interface, variations in physical characteristics causing crack production and propagation at the interfaces, and eventually disrupting the integrity of the formed structure [10]. Many different types of studies are being conducted throughout the world on the creation of highly functional bimetallic structures using the WADED technique. WADED has effectively generated a variety of bimetallic structures, and the interfacial phenomena have been studied. Ahsan et al. [11] fabricated SS316L to IN625 bimetallic structure using the CMT-WADED process. FCC crystal growth in the $\langle 001 \rangle$ direction was observed across the interface, and a large quantity of δ ferrite and laves phase on the SS316L and IN625 sides were detected. The ultimate tensile strength (UTS) was observed to be similar to the WADED SS316L, and the bimetallic structure fails from the SS316L side. Moreover, an increased elongation of 40%, the 200% of the as-deposited SS316L, was attributed to increased ductility. Zhang et al. [2] developed SS316L and copper bimetallic structure using an IN718 interlayer without metallurgical defects and cracks. The Cu area of the SS-IN718-Cu tensile specimens fractured while the interiors remained intact, showing that the interfacial bonding strength exceeded the Cu UTS (257 ± 25 MPa). 125% increase in thermal conductivity was noticed as compared to steel. Furthermore, numerical modelling showed no excessive residual stresses were detected across the interface. Singh et al. [12] developed NiTi-SS316L bimetallic structure using the WADED process. At the NiTi-SS joint interface, brittle intermetallic compounds such as TiCr_2 , FeNi, NiTi, TiNi_3 , and Ti_2Ni were observed. Also, the joint's maximum compression strength is 570 MPa, and the joint's breakage occurs at the fusion zone on the NiTi alloy side, confirming that it is the weakest zone. Moreover, Sridar et al. [13] did interfacial characterisation of P91 steel and IN740H bimetallic structure fabricated using the WADED process. Intergranular cracks with NbC (niobium carbide) were observed in the gradient zone, and the gradient zone was found to be ~ 2200 μm . Microhardness was lower for the gradient zone than for the P91 steel and IN740H sides. Although many researchers have published various combinations of bimetallic structures using the WADED process, the characteristics of Ti6Al4V-IN718 dissimilar structures

developed using WADED are not yet known. The bimetallic structure of these materials, high-strength alloys utilised in various extreme applications, may be used in numerous aircraft applications. Commonly, it is considered that aerospace components have complex geometry, difficult-to-machine parts, high buy-to-fly ratio, small production runs, and high performance. Moreover, the density of Ti-alloy is roughly half that of Ni-superalloys; hence adopting such material combinations can result in considerable weight reductions for aerospace components like engine combustion chambers, channel-cooled rocket nozzles, acoustic liners in subsonic jet engines, etc. In fabricating such bimetallic structure, due to the challenge of controlling the various detrimental intermetallic phase formation (i.e., NiTi, Ni_2Ti , and NiTi_3) at the diffusion interface, it is very difficult to maintain the structural integrity between Ti6Al4V and IN718. This study demonstrates the development of Ti6Al4V and IN718 bimetallic structure using CuSi interlayer as the diffusion barrier or metallurgical adhesive to hinder the inter elemental diffusion of titanium and nickel across the interface to enhance the functionality of bimetallic structure. Moreover, inspired from the high entropy alloy formation mechanism, Cu-powder was also introduced along with CuSi interlayer to increase the entropy of the Cu-Ti interface to avoid the formation of detrimental intermetallic. The final structure was characterised further for microstructure, elemental distribution, interfacial phase formation kinetics, tensile properties, and hardness profile. This study provides a novel approach for the development of Ti6Al4V and IN718 bimetallic structure using WADED process.

2 Materials and Experimental Procedure

2.1 Materials

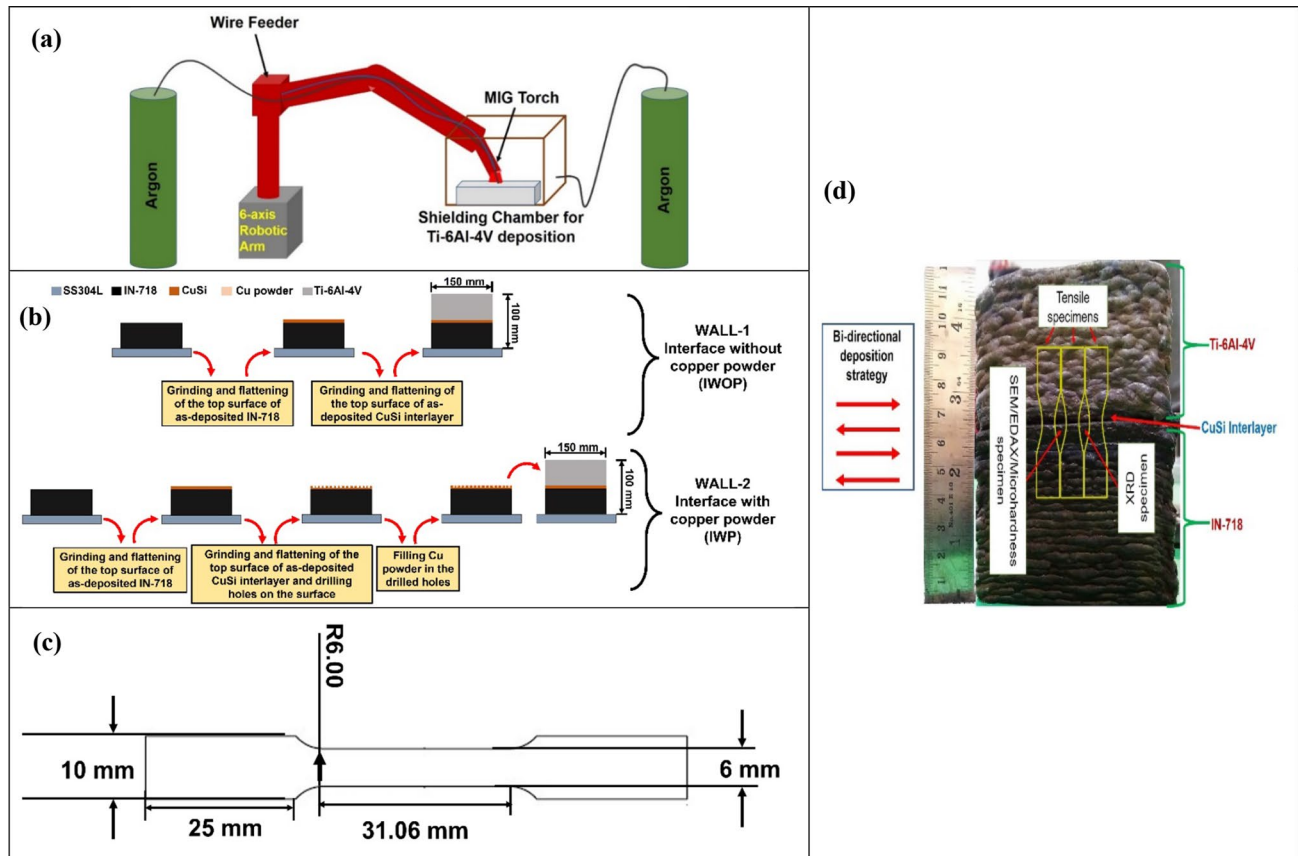
Ti6Al4V, IN718, and CuSi wires of a diameter of 1.2 mm are used feedstock for the deposition process. An SS304L plate of dimension 200 mm \times 150 mm \times 15 mm was used as a substrate for the deposition of the IN718-Ti6Al4V bimetallic wall structure using CuSi as an interlayer. The composition table for the Ti6Al4V (ER Ti-5), IN718 (ERNiFeCr-2), CuSi (ER-CuSi A), and SS-304L is shown in Table 1.

2.1.1 Experimental Procedure

The deposition process is carried out with a 6-axis articulated robotic arm (Make: ABB, Model: IRB1520ID) and an inert metal gas (MIG) power source (Make: Fronius, Model: TPS320i). The MIG-WADED system utilised for the deposition is shown in Fig. 1a. In the beginning, IN718 was kept at the bottom, followed by two layers of CuSi interlayer, and finally Ti-6Al-4V at the top, to create two

Table 1 Elemental composition summary of materials used (wt%)

Material	Composition											
SS304L	C	Si	Mn	P	S	Cr	Ni	Mo	Cu	Nb	Al	
	0.079	0.2858	0.8	0.0032	0.0194	18.56	8.2002	0.2654	0.2920	0.0281	0.003	
Ti6Al4V	Ti	V	Al	C	O	Fe	N	Y	H	–		
	(89.5)	(3.81)	(6.28)	(0.013)	(0.12)	(0.18)	(0.018)	(<0.005)	(0.0029)			
IN718	Ni	Mo	Al	Fe	Nb+Ta	Cr	Ti	Mn	–			
	52	3	0.50	19	5	18	0.90	0.085				
CuSi	Cu	Si	Fe	Al	Mn	–						
	93.99	4.0	0.50	0.01	1.50							

**Fig. 1** a Schematic representation of setup used. b Schematic illustration of deposition strategy, c Tensile sample dimension, d As-deposited bimetallic wall structure

walls. The addition of copper powder makes the walls different from one another. At the Cu-Ti interface, one wall has just CuSi, which is known as an interface without copper powder (IWOP), whereas the other wall is CuSi + copper powder which is known as an interface with copper powder (IWP). These two walls were deposited using similar process parameters shown in Table 2. Despite the similarity, one wall was incorporated with pure Cu powders at the Cu-Ti interface to increase the entropy of the Cu-Ti interface, which may diminish the intermetallic formation [14]. A total of 25 holes diameter of 3 mm and depth of 3 mm, were drilled on

the Cu interlayer at equal intervals and filled with Cu powder (~45 μm) before the Ti-6Al-4V deposition. The height and length of both as-deposited walls were kept at ~100 mm and ~150 mm, respectively.

For a better understanding of the deposition procedure, a schematic diagram is shown in Fig. 1b. Figure 1d depicts the deposition path taken along with the as-deposited wall structure. To determine the ideal deposition parameter of Ti-6Al-4V over CuSi, the Cu-Ti interface produced via the WADED method was examined early [15]. Table 2 displays the process parameters used for the deposition. The

Table 2 Process parameter selected for the deposition of bimetallic structure

Input parameters	Values
<i>For Ti6Al4V</i>	
Deposition current (A)	70
Travel speed (mm/s)	6
Voltage (V)	20
<i>For IN718</i>	
Deposition current (A)	191
Travel speed (mm/s)	9
Voltage (V)	22.7
<i>For CuSi</i>	
Deposition current (A)	91
Travel speed (mm/s)	5.8
Voltage (V)	20
Arc efficiency (η)	0.85
Heat input (J/mm) at Ti6Al4V/CuSi interface	198.3
Shielding gas at the torch	99.99% pure Argon
Shielding gas at the chamber	99.99% pure Argon
Gas flow rate at the deposition torch	20 LPM
The gas flow rate in the shielding chamber	25 LPM
Contact tip to workpiece distance	11–13 mm

parameters for the deposition of IN718 and copper alloy are selected from the previous research by Raja et al. [16] and Baby et al. [17], respectively. The deposition of the first four layers was performed by keeping the factor of low heat input into account. The intermetallic formation at the bimetallic interface depended on the heat input [18]. As the heat input increases, the diffusion across the interface increases and this increase in the heat input give rise to the interfacial cracking phenomenon. Higher intermetallic thickness (IMT) is more prone to interfacial cracking under cyclic thermal gradient and extreme condition.

Moreover, during the experiment, it was noticed that the sharp cooling gradient of the interface generated cracks as the crackling sound was obtained from the deposited Cu–Ti interface during cooling. Therefore, a strategy has been developed under which the first four layers of Ti over the Cu interlayer were deposited, considering the parameters mentioned in Table 2. After the 4th layer, the input current was increased to 1.5 times the previous one, so the heat transferred through conduction let the interface cool down. In addition, there was no time delay between two consecutive layers of titanium deposition to avoid the development of a sharp cooling gradient at the Cu–Ti interface. Furthermore, to ensure oxide-free titanium deposition, additional shielding is provided to the titanium deposits in addition to the torch shielding. The shielding environment was maintained at 150 ppm oxygen content measured by Weld Purge Monitor (Make: Huntingdon Fusion Techniques Model: Argweld

Purge Eye 300 nano) inside an airtight chamber using a controlled argon gas flow from a different cylinder.

2.1.2 Metallurgical and Mechanical Characterisation

The samples for various characterisations were extracted from the wall, as shown in Fig. 1c. Two vertical pieces between the three tensile samples were extracted from the wall for scanning electron microscopy (SEM), energy dispersive x-ray spectroscopy (EDAX), X-ray diffraction (XRD), and micro-hardness. The samples were ground and evenly polished with sandpapers ranging in grit size from 180 to 2500, followed by cloth polishing with a diamond paste ranging from 0.5 to 1 μm . Kroll's reagent (HNO_3 + distilled water + HF) for Ti–6Al–4V, Kalling's no. 2 reagent (CuCl_2 + HCl + Ethanol) for IN718, and copper no. 1 reagent (HNO_3 + distilled water) for ER-CuSi, are used to etch the polished samples preferentially. The etched samples were viewed in the SEM (Make: Carl Zeiss; Model: Gemini SEM300) and EDAX (Make: Oxford). Then, using a 600 W X-ray source and a Hypix-400 MF 2D hybrid pixel array detector (HPAD), a Rigaku Miniflex XRD system gathered X-ray diffraction (XRD) patterns across samples that were 10 mm \times 10 mm \times 5 mm in size. A scan rate of 10° per minute was used for analysis in the Smart Lab Studio-II program.

Furthermore, the tensile testing was performed on ASTM E8 (sub-size) specimens as shown in Fig. 1c extracted 3 in number from each wall. The gauge section of the specimen contains Ti–Cu–Ni alloy sections. The tensile testing was performed on universal testing equipment (make: Tinius Olsen; model: H50 KS) with a strain rate of 0.04 min^{-1} . Along the build direction, the microhardness of the deposited structure is measured. The distance between two successive indentations is measured as one millimetre. With a 100-gf load and a dwell duration of 10 s, the Vicker's microhardness testing apparatus (manufacturer: Innovatest; model: Anova Falcon 500) was used.

3 Result and Discussion

3.1 Metallographic Characterisation

The metallography obtained at various positions of the deposited wall is shown in Fig. 2. The deposition of Ti–6Al–4V at the top of the structure in Fig. 2a showed two-phased structures, i.e., needle like α + β -phase (martensite) and primary α -phase, in both deposited walls. Such structure forms when the Ti–6Al–4V alloy rapidly cooled from greater than 1050 °C temperature [19]. Due to rapid cooling from such a high temperature and availability of copper sink at the base, the α -phase could not able to completely

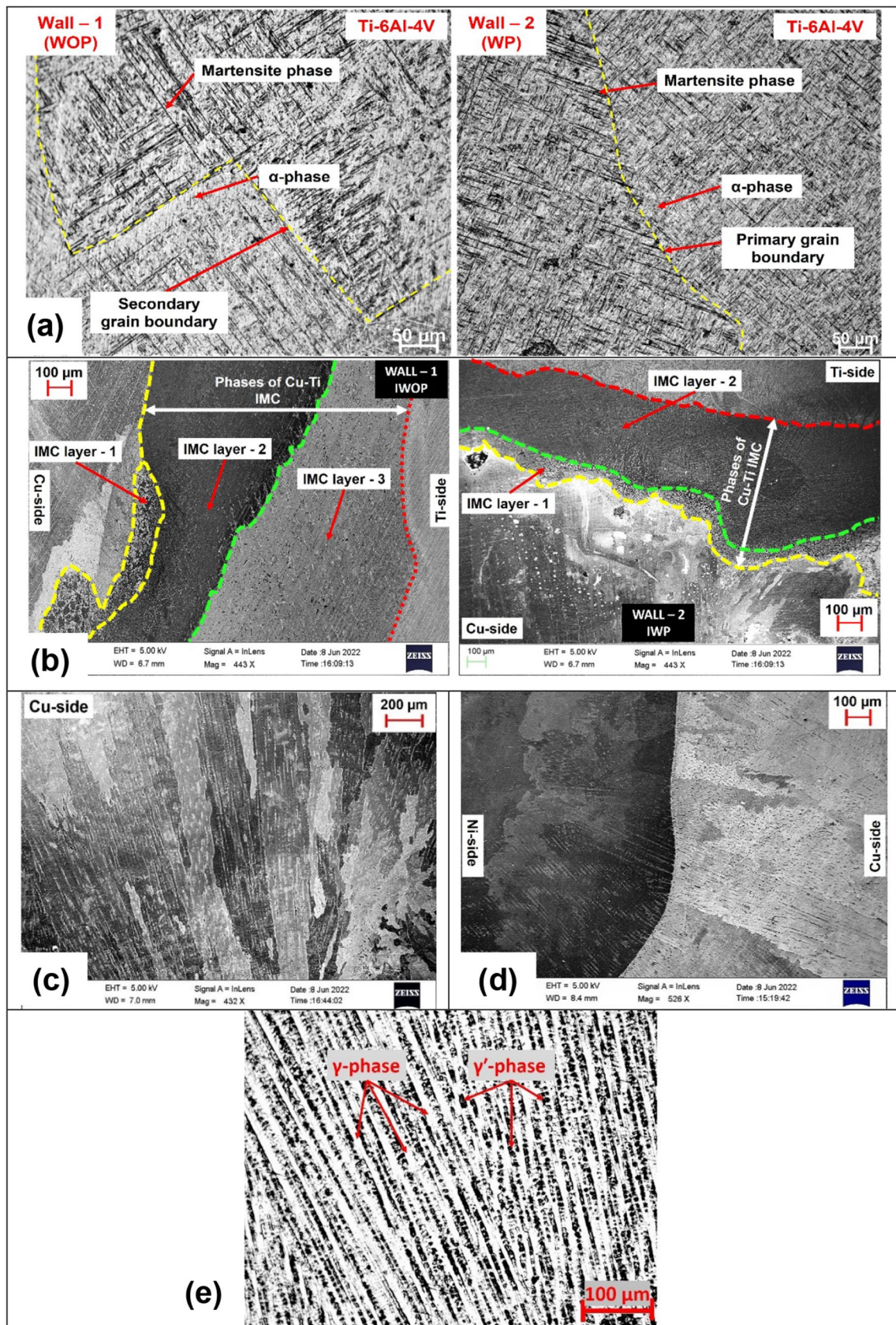


Fig. 2 a Microstructure obtained at Ti-side. b Cu–Ti interface of both deposited walls. c Cu-side. d Ni–Cu interface, e Ni side

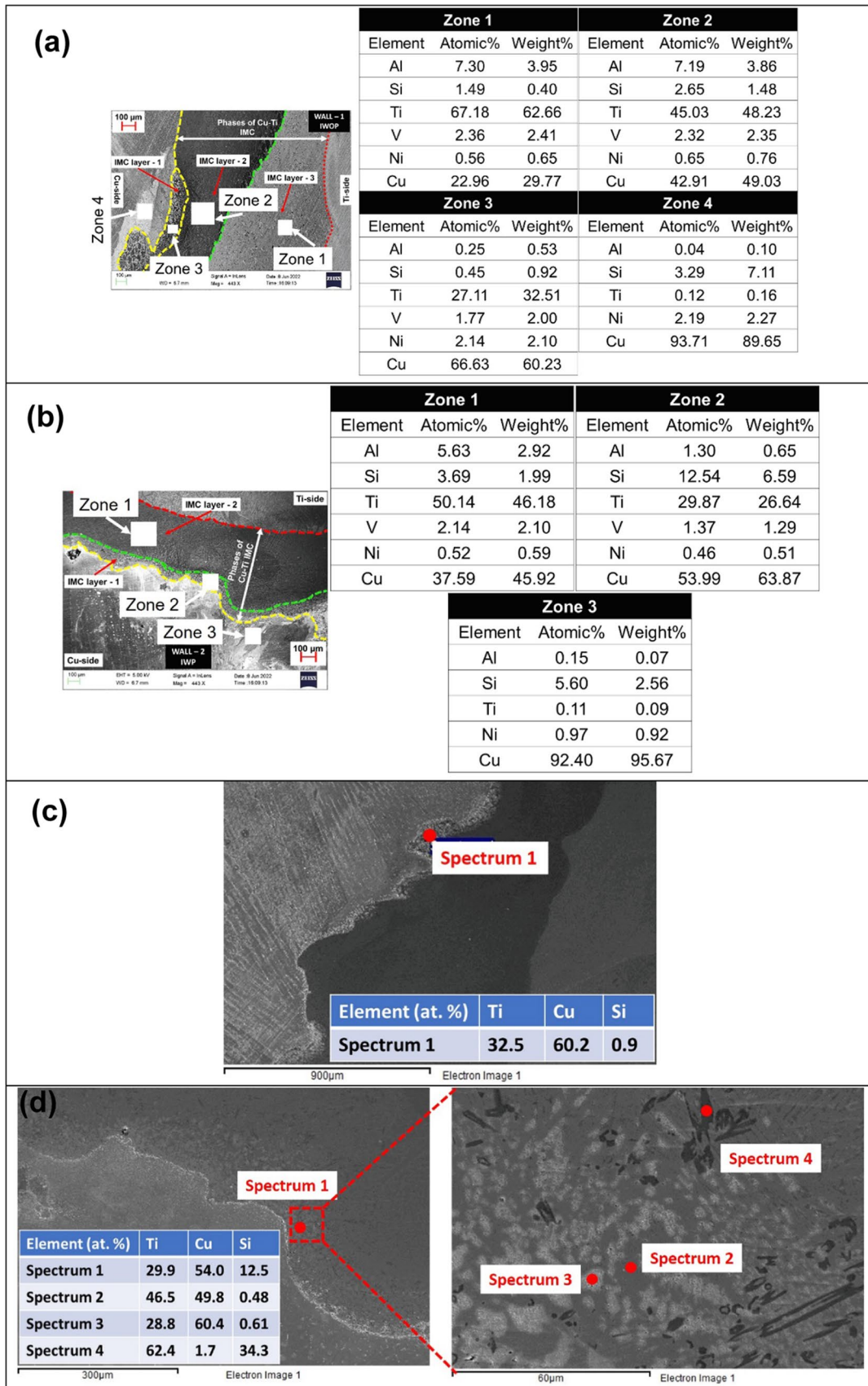


Fig. 3 EDAX area scan **a** Cu–Ti interface of WOCP. **b** Cu–Ti interface of WCP. **c** Non-confirmation of Ti_5Si_3 at IMC layer-1 of IWOP, **d** confirmation of Ti_5Si_3 at IMC layer-1 of IWP

transformed into to β -phase and, hence, retained at room temperature. Equation (1) illustrates how the eutectoid reaction led to the $\alpha + \beta$ -phase transformation after the transition temperature of 975 °C [20] and Eq. (2) depicts the β -phase to α -phase transition at 1050 °C [19].



The rapid transformation of α' -Ti to β -Ti and then into $\alpha + \beta$ Ti is followed by a gradual transformation back into α -Ti. The martensite phase precipitating in the matrix causes strengthening at room temperature. However, the α -phase fraction results in a trade-off between strength at high temperatures and more significant flow stress at high temperatures. In the deposited structure, the α -Ti was found nearly 65.76% and 66.12% of the wall without powder and the wall with powder, respectively. This shows that the deposited structure will have ample strength at room and high temperatures to be used in structural application [21]. Moving towards the Cu–Ti interface, no cracks have been found at the interface, which justifies the effective strategic deposition of Ti over the Cu interlayer for both walls, i.e., a wall without powder and a wall with powder shown in Fig. 2b. However, the Cu–Ti interface without powder (IWOP) shows three distinctive layers of intermetallics.

In contrast, the interface with powder (IWP) shows only two distinctive layers of intermetallic phases with the less interfacial thickness (~360 μm) compared to the interface without powder (~535 μm). This suspects the presence of some phase kinetics, which inhibited intermetallic phase growth at the Cu–Ti interface without a powder sample. The CuSi interlayer shows its traditional columnar structures with Si precipitated at the interdendritic regions of Cu in Fig. 2c. The addition of Si in Cu improves both strengths and ductility [22], imparts the proper cushioning effect to the thermal stresses developed at the Cu–Ti interface and assures the intactness between Cu and Ti. On the other hand, the Cu and Ni, which have atomic numbers 29 and 28, respectively, are next to one another on the periodic table. The two substances are entirely miscible in their liquid and solid states and are closely linked [23]. Cu–Ni alloys crystallise in a face-centred cubic lattice across the whole concentration range; hence, there will be no chance of forming secondary detrimental phases. The as-deposited Cu–Ni interface in both walls looked perfect in terms of bonding, and no such secondary phases were noticed at the interface, as shown in Fig. 2d.

Moreover, a smooth transition between Ni and Cu has been noticed, moving Ni to Cu. The Ni dendrites directly diffuse into Cu and develop a continuous columnar dendritic

growth across the Ni to Cu. The IN718 shows its conventional cellular microstructure with γ -phase and interdendritic precipitant, γ' -phase, as shown in Fig. 2e. The intermediate phase fraction of the γ' -phase is found at nearly 33.9% and 34.2% in the wall with powder and without powder, respectively. IN718 is a precipitation hardening alloy in which the pure Ni is called γ -phase, whereas the intermetallic secondary precipitant, i.e., $\text{Ni}_3(\text{Nb}, \text{Ti}, \text{Al})$, is called γ' -phase [23]. Therefore, the presence of γ' -phase in adequate amounts will improve the strength of the alloy extensively without appreciable depreciation in ductility. The as-deposited IN718 shows a suitable quantity of γ' -phase to produce excellent strength in the material. Looking back at all of the materials and their interfaces along with their probable phase analysis, the Cu–Ti interface looks much more vulnerable to fracture during loading due to continuous and incoherent Cu–Ti intermetallic phases. This phenomenon makes the Cu–Ti interface a more important region to be studied further for the highly functional Ni–Cu–Ti trimetallic structure.

3.1.1 EDAX Analysis and Phase Formation Kinetics at the Interfaces

3.1.1.1 Cu–Ti Interface The intermetallic compound (IMC) in the layered form experienced the EDAX scan at the interface, as shown in Fig. 3. The area and point scans were performed at the interface without copper powder (IWOP) and interface with copper powder (IWP), as shown in Fig. 3a, b. The elemental fraction of Cu and Ti was compared with the Cu–Ti phase diagram and concluded the formation of Ti-rich $\text{CuTi} + \text{CuTi}_2$ phase in zone-1 and $\text{Cu}_4\text{Ti}_3 + \text{Cu}_3\text{Ti}_2$ phase in zone-2, whereas $\text{Cu}_4\text{Ti} + \text{Cu}_3\text{Ti}_2$ in zone-3 for the IWOP sample. However, at zone-1, the fraction of CuTi would not be significant as the iso-concentration line in zone-1 lies much closer to the CuTi_2 phase. For IWP, there exist only two layers of intermetallic phases at the interface. The area scan at zone-1 indicated the formation of the $\text{Cu}_4\text{Ti}_3 + \text{Cu}_3\text{Ti}_2$ phase, whereas zone-2 indicated the formation of $\text{Cu}_4\text{Ti} + \text{Cu}_3\text{Ti}_2$ phases. Comparing the EDAX elemental distribution of the Cu–Ti interface for IWOP and IWP regions, the IWOP has an additional layer of CuTi_2 intermetallic. This was undoubtedly incurred due to the diffusion of Cu at a considerable distance where the Ti-rich Cu–Ti intermetallic formed. The other sample, IWOP, did not show such diffusion behaviour of copper, despite the same deposition parameters. Observing deep down into the Cu–Ti interface of the IWP sample, some traces of Ti_5Si_3 were noticed at the IMC layer-1 (zone-2 region); however, such disilicide was not effectively traced at the IWOP, as shown in Fig. 3c and d despite both deposition contain same Ti–Si composition. This typical occurrence could be related to entropy, which measures randomness and rises as entropy increases. In contrast to the solid

interlayer in IWOP, the Cu powder added to the IWP interface obviously increases randomness and may therefore have a higher entropy. Accordingly, the formation enthalpy ($\Delta H = \Delta G + T \cdot \Delta S$) of Cu–Ti intermetallics also increases at the IWP wall. The diffusivity of Cu in Ti is in order of $3.8 \times 10^{-5} \text{ m}^2/\text{s}$ [24] whereas the diffusivity of Si in Ti is in order of $7.5 \times 10^{-14} \text{ m}^2/\text{s}$ [25], which indicates that the diffusion of Cu in Ti is much faster than Si in Ti. Therefore, in the case of IWOP, the Cu reaches Ti in a much faster manner, resulting in the formation of various Cu–Ti IMCs, and Si is prevented from entering Ti and forming Ti–Si IMCs as a result. However, in the case of IWP, Cu powder is introduced at the interface to increase the enthalpy of Cu–Ti IMCs. As a result, during the melting process, Ti reacts quickly with Cu and may produce a supersaturated solid-solution of CuTi; however, the reaction is incomplete and Cu may be rejected during solidification, which could allow Si to enter in the interstitial positions and result in the formation of the Ti_5Si_3 compound because it has a lower formation enthalpy (-75 kJ/mol) than any other Cu–Ti IMC phase [26]. Furthermore, transition metal silicides, such as nickel silicide [27], copper silicide [28], titanium silicide [29], etc., are known to act as a copper diffusion barrier. Thus, the formation of Ti_5Si_3 at the IWP hindered the Cu diffusion into the Ti, resulting in the lesser IMC layer thickness in IWP than in IWOP.

Conclusively, as Ti is deposited over the Cu interlayer, mixing of Ti and Cu occurs at the interface in a liquid state. As the solidification starts, the CuTi IMC forms first, and more copper diffuses towards the Ti side, whereas more Ti diffuses towards the Cu side. Thus, three distinctive intermetallic zones were created at the interface, i.e., the CuTi zone, Cu(rich)–Ti zone, and Cu–Ti(rich site). However, due to the formation of Ti_5Si_3 , the Cu–Ti (rich) IMC layer is not found at IWP. With the further decrease in temperature, the CuTi transformed into Cu_4Ti_3 and Cu_3Ti_2 [30]; meanwhile, CuTi₂

IMC formed at Ti(rich zone) and $\text{Cu}_4\text{Ti} + \text{Cu}_3\text{Ti}_2$ formed at Cu rich zone. The general transformation sequence of CuTi IMC follows as $\text{CuTi} \rightarrow \text{Cu}_4\text{Ti} \rightarrow \text{Cu}_4\text{Ti}_3 \rightarrow \text{CuTi}_2$ [30]. It should be noted that the given heat input during the deposition favoured the complete transformation of CuTi into Cu_4Ti ; however, it was not found enough to establish the total change of Cu_4Ti into Cu_4Ti_3 at the Cu(rich)–Ti zone, which led to precipitation of Cu_4Ti into the $\text{Cu}_4\text{Ti}_3 + \text{Cu}_3\text{Ti}_2$ matrix. Since there is no Ti(rich zone) at IWP, thus no traces of CuTi_2 has been observed. To better understand the layer formation at the Cu–Ti interface for IWOP and IWP, schematic diffusion models are shown in Fig. 4.

3.1.1.2 Ni–Cu Interface Ni and Cu are completely miscible metals in liquid and solid solutions. Although Ni and Cu are readily joined in the fusion process, the residual thermal stress may lead to embrittlement and hot cracking [31]. However, the as-deposited Ni–Cu interface did not show any cracks or formation of secondary phases at the interface. A line scan across the interface identifies the diffusion behaviour between the two, shown in Fig. 5. Since the Ni–Cu interface was developed under similar circumstances and deposition parameters for both walls,

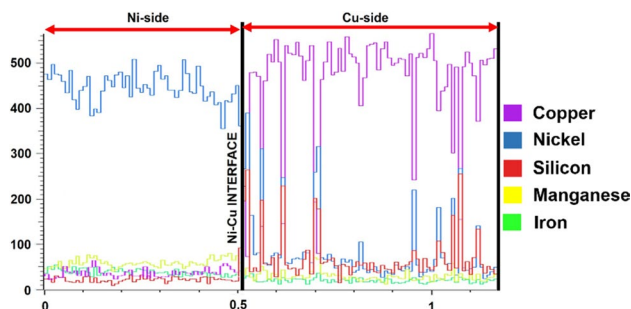
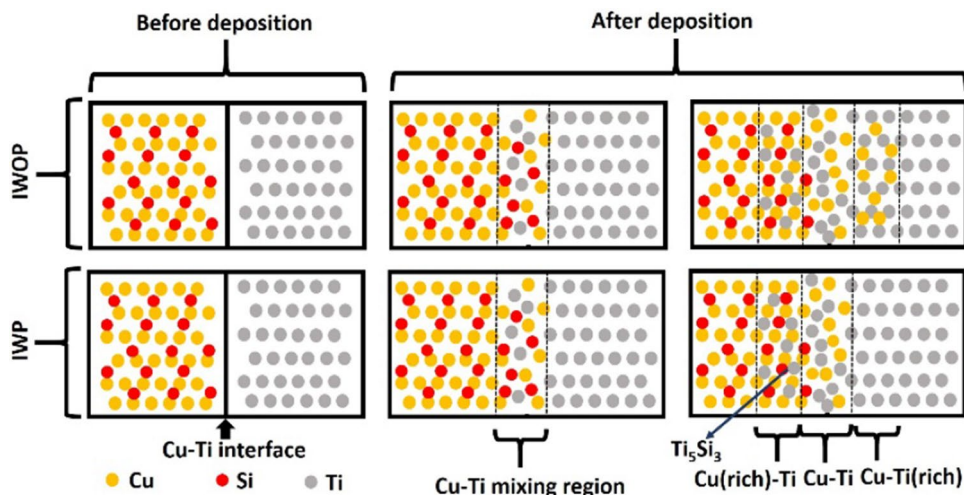


Fig. 5 Line scan at Ni–Cu interface for wall-1 (IWOP)

Fig. 4 Diffusion models for IWOP and IWP



the diffusion behaviour was also the same. The line scan shows a negligible amount of diffused Cu on the Ni side, whereas the Cu side received an ample amount of diffused Ni. This might happen because of the difference in melting point between the depositing and substrate alloy. The melting point of Cu is around 1050 °C, whereas the melting point of Ni is ~1450 °C. Therefore, when Cu was deposited over Ni, only partial Ni melted at the interface. Moreover, it would have been easier for Ni to diffuse into molten Cu rather than diffusion of Cu into solid Ni. Apart from this, due to the unaltered concentration of Cu near the Ni–Cu interface (Cu-side), the segregation of Si did not occur, which avoided the formation of nickel silicides in that region.

It could be also noted that when low melting point materials like Cu are deposited on high melting point materials like Ni, diffusion occurs primarily in the build direction and partial melting of the substrate may result in a thinner mixed Ni–Cu interface region. In contrast, a significant amount of the low melting point substrate (Cu) melts while depositing material with a higher melting point, such as Ti, creating a thicker mixed zone at the Cu–Ti interface and diffusion generally occur towards

build direction. Thus, the position of material with respect to their melting point may have an impact on the interface thickness.

3.1.2 Phase Formation and Kinetics

The XRD analysis of the Ni–Cu and Cu–Ti interfaces of the as-deposited IWOP and IWP walls revealed the same intermetallic phases encapsulated by EDAX analysis of IWOP and IWP. The Cu_4Ti_3 , Cu_3Ti_2 , Cu_4Ti , and CuTi_2 intermetallic phases are detected during the XRD analysis of IWOP and IWP, except a different phase is noticed in the IWP, i.e., Ti_5Si_3 as shown in Fig. 6a and b. This section discussed various phase formation and transformation kinetics at Cu–Ti and Ni–Cu interfaces.

As discussed in Sect. 3.1.1, the first phase, which forms due to its low formation enthalpy and higher stability, is CuTi in both samples at the Cu–Ti interface at around 989 °C. The chances of the formation highly non-stoichiometric phase (i.e., Cu_4Ti) are high after the CuTi formation. The formation enthalpies of CuTi and Cu_4Ti are -11.12 kJ/mol and -5.53 kJ/mol, respectively. Instead of the significant differences in the formation enthalpies, the driving

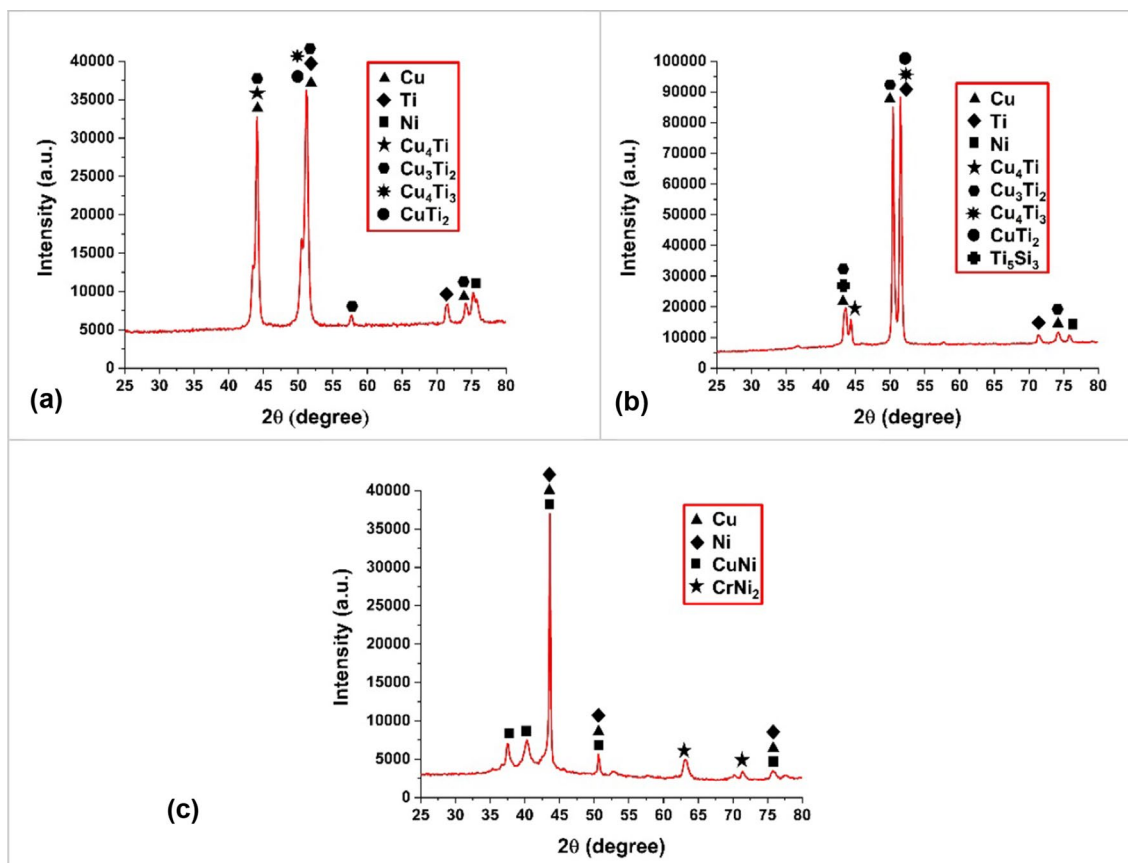
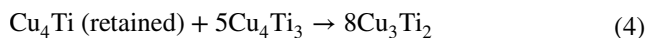
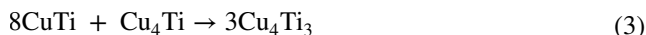


Fig. 6 XRD pattern **a** for IWOP, **b** for IWP, and **c** for the Ni–Cu interface

force (ΔG) for the formation of Cu_4Ti is ~ 510 J/mol closer to the $\text{Cu}_4\text{Ti}_3 \sim 510$ J/mol. However, it is also very difficult to form a stoichiometric phase during continuous mixing of Cu–Ti at a high temperature of around 890°C . This increases the probability of forming Cu_4Ti after CuTi at the Cu–Ti interface. The metastable nature and solid-state diffusion of Cu_4Ti with the most stable phase (i.e., CuTi) lead to further transformation of it into Cu_4Ti_3 . The transformation reaction of Cu_4Ti into Cu_4Ti_3 is shown by Eq. (3) [30]. The high cooling rates during the initial layers of deposition hindered the complete transformation of CuTi and Cu_4Ti . The retained Cu_4Ti at the interface further reacts with formed Cu_4Ti_3 to give Cu_3Ti_2 during the subsequent layers as the interfacial temperature at a particular deposition layer turn higher enough for solid-state diffusion. Moreover, the transformation reaction of Cu_4Ti and Cu_4Ti_3 is shown by Eq. (4) [30].



The XRD results showed no presence of CuTi at the interfaces of both the samples, as shown in Fig. 6a and b. This offers a complete transformation of CuTi into the subsequent phases. Further, as discussed in Sect. 2.2, there was no time delay between two consecutive layers of titanium deposition to avoid the development of a sharp cooling gradient at the Cu–Ti interface. This slowing of the cooling gradient results in late nucleation of CuTi and Ti at a lower temperature of around $750\text{--}780^\circ\text{C}$ resulting in the formation of the CuTi_2 phase of Cu–Ti intermetallic. A similar phenomenon was reported by Laik et al. [30] at the CuTi/Ti interface due to late nucleation.

Apart from the Cu–Ti interface, the Ni–Cu interface was also analysed with the XRD technique. However, the XRD peaks obtained at the Ni–Cu interface for IWOP and IWP walls are also identical due to similar process parameters and strategies. Therefore, XRD peaks of the Ni–Cu interface for the IWOP wall are only shown in Fig. 6c. The equiatomic CuNi phase has been observed at the interface due to the miscibility gap between Cu and Ni phases. A miscibility gap is a region of a phase diagram between two highly miscible elements in a certain temperature region [32]. For CuNi equiatomic phase, Iguchi et al. [32] determined that the miscibility gap formed at 527°C . Due to the high conductivity of Cu, rapid solidification at the interface took place, which led the CuNi phase to freeze and remain untransformed in the matrix.

Moreover, another phase is noticed in the XRD analysis, i.e., CrNi_2 . However, this phase is not generally seen in the Ni–Cr–Mo alloys because of its less stability and low temperature of formation, i.e., 590°C [33]. Verma

et al. [32] reported that less content of Ti and W in the alloy leads to the formation of the D0_{22} crystal structure type CrNi_2 intermetallic phase. Since IN718 does not have W content and a small amount of Ti may have diffused towards the Cu, Ti has many affinities for Cu compared to Ni. Thus, during the heating and cooling cycle, as titanium started moving towards the Cu matrix, the Cr attacked the Ni matrix after reaching the composition to form the CrNi_2 phase. The CrNi_2 phase precipitated very small at the Ni–Cu interface, which may increase the interfacial strength between the two as it will pin the dislocation line during the deformation.

3.2 Mechanical Characterisation

3.2.1 Tensile Testing and Fractography

During the tensile test, it was found that the samples of IWOP and IWP walls fractured in the vicinity of the Cu–Ti interface (on the Ti side). The engineering stress–strain curves obtained for samples IWP and IWOP are illustrated in Fig. 7. The 0.2% proof stress (PS) values for IWOP and IWP are found at 36.43 ± 5.02 MPa and 16.09 ± 1.15 MPa, respectively. Furthermore, the ultimate tensile stress (UTS) for IWOP and IWP are 152.31 ± 40.74 MPa and 32.51 ± 11.97 MPa. Despite using the same process parameters, a significant difference in PS and UTS can be noticed between the IWOP and IWP samples. Thus, the copper powder in the IWP sample generates the metallurgical orientation towards reduction in tensile strength by catalysing detrimental intermetallic compounds at the interface. The presence of copper powder at the Cu–Ti dissimilar interface catalysed the formation of highly brittle Ti_5Si_3 at the interface (on the Ti side). Ti_5Si_3 at the interface not only impedes the diffusion of EDAX Cu towards the Ti but also inhibits the elongation during the deformation. This means that the work-hardening effect after the yield point is not observed in the case of IWP. However, the IWOP samples show significant elongation ($> 6\%$) to be considered ductile compared to IWP samples. Therefore, during the deformation of IWP samples, the strain-induced transformation may occur at the Cu–Ti different interface, increasing the strength. To prove this hypothesis, the SEM and EDAX analysis has been performed on the fractured surfaces of both IWOP and IWP samples.

The SEM images of fractured surfaces have been captured, as shown in Fig. 7c and d. The fracture mode can be assessed as brittle as a river bed-like pattern is noticed on the fracture surfaces of both IWOP and IWP samples. In the brittle fracture, the crack propagates rapidly with sound speed and often propagates by cleavage. The cleavage breaks an atomic bond along a specific crystallographic

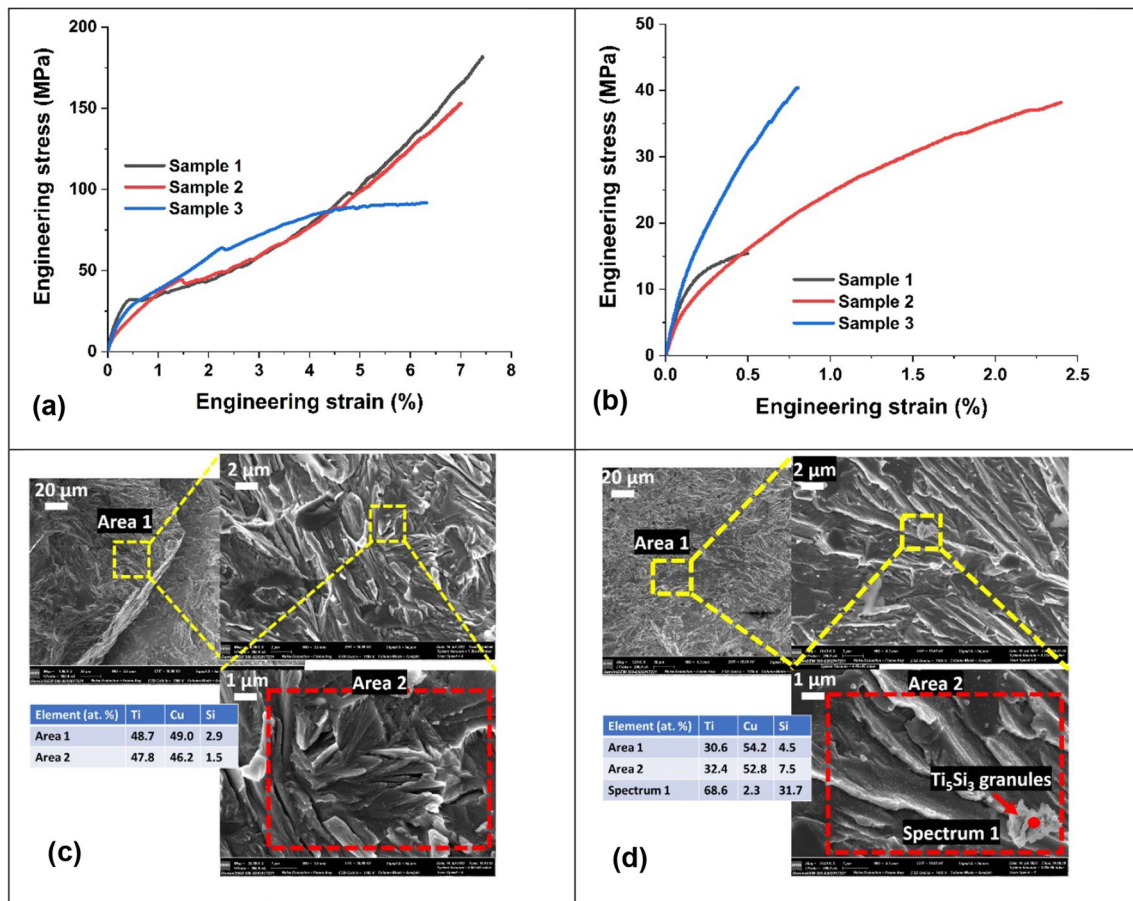


Fig. 7 Engineering stress versus Engineering strain curves for **a** IWOP, **b** IWP; EDAX scan of fractured surface for **c** IWOP and **d** IWP samples

plane, also known as the cleavage plane. Because the cleavage planes in various grains are oriented differently, the texture of the fracture surface is faceted. The nature of brittle fracture is transgranular in both IWOP and IWP samples; however, the intergranular fracture is also noticed in the IWP samples, as shown in Fig. 7d. The intergranular fracture generally occurs when the grain boundaries are weaker than the grain itself. Thus, the intergranular fracture weakened the grain boundary due to the precipitation of Ti_5Si_3 . The EDAX analysis reveals the availability of the CuTi IMC phase in IWOP samples. In contrast, no trace of the CuTi phase is noticed on the fractured surface of IWP samples. This means that, in IWOP samples, the strain-induced transformation of Cu_4Ti_3 , Cu_3Ti_2 , and $CuTi_2$ phases into a highly stable CuTi phase [30] occurred. However, no strain-induced transformation of less stable Cu–Ti phases into CuTi phases is observed in the samples of IWP during deformation. Apart from this, traces of Ti_5Si_3 were also noticed on the facets of the transgranular fracture. This concludes that the presence of Ti_5Si_3 impedes the diffusion of Cu into Ti, imparts more brittleness to the Cu–Ti matrix, inhibits the transformation

of less stable Cu–Ti phases into highly durable CuTi IMC phase, and finally decreases the strength and elongation during tensile deformation.

3.2.2 Micro-hardness Testing

The microhardness was measured from the Ni side towards the Ti side along the build direction, including the Cu-interlayer, as shown in Fig. 8. The indentations were taken at both sides (i.e., 10 mm on both sides) of the Cu–Ti interface. It was found that the Ni side shows the hardness values ranging from 195 to 240 HV for IWOP and 190–245 HV for IWP deposited structures which are typical for additively manufactured deposited IN718 [34], as there was no infusion of Cu-atom found on the Ni-side (shown in Fig. 8c). The hardness value in the CuSi layer was observed to be 98–156 HV for IWP and 120–137.2 for IWOP. This increase in the hardness value of the copper was due to the distribution of Ni-atom on the Cu side, as shown in Fig. 8c. The hardness value was not found to be stabilised (i.e., IS 14811:2000) within the copper because of the thickness of the CuSi layer (i.e., 3–4 mm thickness of the two layers). The hardness was increased in the region away

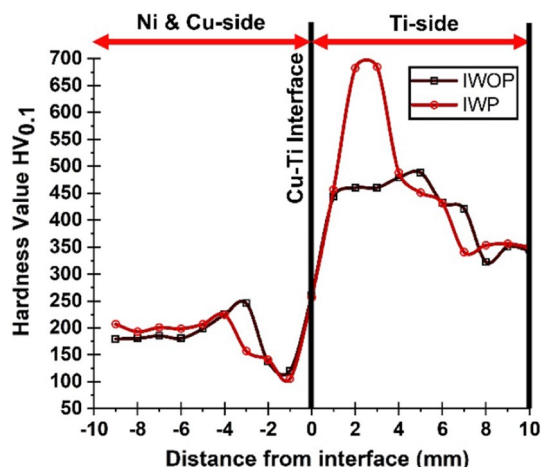


Fig. 8 Micro-hardness profile from IN718/CuSi/Ti6Al4V

from the CuSi towards the Ti–6Al–4V due to the formation of various IMC at the Cu–Ti interfacial region. The hardness value increases to ~680 HV in the IWP structure and ~485 HV in the IWOP structure. The increase in the hardness depends on the composition of CuTi and CuTi₂ in the dual-phase IMC observed in the interfacial region, as shown in Fig. 4a. Zhu et al. [35] reported that the CuTi IMC has the highest hardness in the Cu–Ti IMC family, i.e., 11.7 GPa, which corresponds to ~1193 HV, whereas, CuTi₂ has ~800 HV (i.e., 7.85 GPa). Since multi-phase Cu–Ti intermetallic formation was observed in this work, the hardness values at the interface are now almost equivalent to the average hardness values of the phases present at the interface. The interfacial hardness is highest for IWP structures and minimum for IWOP structures. However, a proportion of CuTi impacts the interfacial hardness as the increase of CuTi fraction increases the interfacial region. The fraction of Cu and Ti in various zones is shown in Fig. 3a and b. The composition indicates the formation of CuTi + CuTi₂ dual IMC phases at the zones in the interfacial region. Using lever rule, the fraction of CuTi in the whole phases of IMC can be calculated as 25%–40% for various zones in IWOP whereas at IWP interfacial region the fraction reaches as high as 75%–90%. Therefore, the more fraction of CuTi in the interfacial region of IWP structure may increase the brittle nature at the interface which can also be validated by the hardness value reached ~680 HV. Hence, the formation of a coherent and less brittle combination of CuTi + CuTi₂ IMC at the dissimilar interface as a result of fabricating a Ti–6Al–4V/IN718 dissimilar structure through the WADED process without copper powder will certainly result in the development of a highly functional Ni–Ti bimetallic structure.

4 Conclusion

Bimetallic structures of Ti–6Al–4V and IN-718 have been successfully fabricated using wire-arc additive manufacturing with improved functionality. The structure seems to be with no interfacial cracking in various micrographs. Hereafter, the mechanical behaviours were analysed, and the following conclusions could be drawn from the work:

- Microstructure on the Ti–6Al–4V two-phased structures, i.e., needle like $\alpha' + \beta$ -phase (martensite) and primary α -phase, in both deposited walls with no interfacial cracking at the Cu–Ti interface and precipitation of Si at the interdendritic region. However, Ni-side showed its conventional cellular microstructure with γ and γ' -phases. Phase fraction of the γ' -phase is found at nearly 33.9% and 34.2% in the wall with powder and without powder, respectively. Moreover, intermetallic thickness (IMT) was decreased to ~360 μm from ~535 μm for Cu–Ti interface with copper powder (IWP).
- EDS analysis confirmed the higher diffusion of Cu towards the Ti-side in the interface without copper powder (IWOP) sample, which results in the formation of three intermetallic layers, i.e., (Zone 1) CuTi + CuTi₂, (Zone 2) Cu₄Ti₃ + Cu₃Ti₂, and (Zone 3) Cu₄Ti₃ + Cu₃Ti₂ as per the atomic composition. However, IWP showed two layers of intermetallic region i.e., (Zone 1) Cu₄Ti₃ + Cu₃Ti₂ and (Zone 2) Cu₄Ti + Cu₃Ti₂. Moreover, diffusion of Ni in Cu is larger than Cu in Ni due to the significant difference in melting point at the Ni–Cu interface.
- Furthermore, the XRD result showed the absence of the most brittle CuTi intermetallic phase at the Cu–Ti interface for both samples. Moreover, a small amount of CrNi₂ precipitated at the interfacial region of Cu–Ni.
- Both samples observed a brittle fracture of tensile samples on the Ti-side near the Cu–Ti interface. The 0.2% proof stress (PS) and ultimate tensile stress (UTS) values of IWOP i.e., 36.43 ± 5.02 MPa and 152.31 ± 40.74 MPa, are higher than the IWP samples.
- The formation of multi-phase Cu–Ti intermetallic results in a hardness value nearly equal to the average of the phases present. The hardness was ~680 HV in the IWP structure and ~485 HV in the IWOP structure. However, Ni-side hardness lies in the range of 190–245 HV, and for CuSi, it lies between 98 and 156 HV for both samples.

Acknowledgements The authors would like to acknowledge the DST-SERB for the financial support (sanction no. ECR/2018/001250) to conduct the research activities. The authors would also like to

acknowledge Director CSIR-CMERI for providing the opportunity and facilities to conduct the research.

Availability of Data and Material There is no need for a separate archive since the manuscript contains all the details needed to reproduce the work.

Declarations

Conflict of interest The authors declare that they have no known conflicts of interest that could have influenced the research presented in this paper.

References

1. A. Elrefaey, W. Tillmann, Solid state diffusion bonding of titanium to steel using a copper base alloy as interlayer. *J. Mater. Process. Technol.* **209**, 2746–2752 (2009). <https://doi.org/10.1016/j.jmatp.rotec.2008.06.014>
2. X. Zhang, L. Li, F. Liou, Additive manufacturing of stainless steel—copper functionally graded materials via Inconel 718 interlayer. *J. Mater. Res. Technol.* **15**, 2045–2058 (2021). <https://doi.org/10.1016/j.jmrt.2021.09.027>
3. B. Onuike, B. Heer, A. Bandyopadhyay, Additive manufacturing of Inconel 718—copper alloy bimetallic structure using laser engineered net shaping (LENS™). *Addit. Manuf.* **21**, 133–140 (2018). <https://doi.org/10.1016/j.addma.2018.02.007>
4. T.E. Abioye, P.K. Farayibi, P. Kinnel, A.T. Clare, Functionally graded Ni–Ti microstructures synthesised in process by direct laser metal deposition. *Int. J. Adv. Manuf. Technol.* **79**, 843–850 (2015). <https://doi.org/10.1007/s00170-015-6878-8>
5. S. Mohan Kumar, A. Rajesh Kannan, N. Pravin Kumar, R. Pramod, N. Siva Shanmugam, A.S. Vishnu, S.G. Channabasavanna, Microstructural features and mechanical integrity of wire arc additive manufactured SS321/inconel 625 functionally gradient material. *J. Mater. Eng. Perform.* **30**, 5692–5703 (2021). <https://doi.org/10.1007/s11665-021-05617-3>
6. T.A. Rodrigues, N. Bairrão, F.W.C. Farias, A. Shamsolhodaei, J. Shen, N. Zhou, E. Maawad, N. Schell, T.G. Santos, J.P. Oliveira, Steel-copper functionally graded material produced by twin-wire and arc additive manufacturing (T-WAAM). *Mater. Des.* **213**, 110270 (2022). <https://doi.org/10.1016/j.matdes.2021.110270>
7. Y.K. Kim, H. Pouraliakbar, S.I. Hong, Effect of interfacial intermetallic compounds evolution on the mechanical response and fracture of layered Ti/Cu/Ti clad materials. *Mater. Sci. Eng. A* **772**, 138802 (2020). <https://doi.org/10.1016/j.msea.2019.138802>
8. T. Bhujangrao, F. Veiga, A. Suárez, E. Iriondo, F.G. Mata, High-temperature mechanical properties of IN718 alloy: comparison of additive manufactured and wrought samples. *Crystals* **10**, 689 (2020). <https://doi.org/10.3390/CRYST10080689>
9. M.R.U. Ahsan, A.N.M. Tanvir, T. Ross, A. Elsayy, M.S. Oh, D.B. Kim, Fabrication of bimetallic additively manufactured structure (BAMS) of low carbon steel and 316L austenitic stainless steel with wire + arc additive manufacturing. *Rapid Prototyping J.* **26**, 519–530 (2020). <https://doi.org/10.1108/RPJ-09-2018-0235>
10. A.R. Paul, M. Mukherjee, D. Singh, A critical review on the properties of intermetallic compounds and their application in the modern manufacturing. *Cryst. Res. Technol.* **57**, 2100159 (2022). <https://doi.org/10.1002/crat.202100159>
11. M.R.U. Ahsan, X. Fan, G.J. Seo, C. Ji, M. Noakes, A. Nycz, P.K. Liaw, D.B. Kim, Microstructures and mechanical behavior of the bimetallic additively-manufactured structure (BAMS) of austenitic stainless steel and Inconel 625. *J. Mater. Sci. Technol.* **74**, 176–188 (2021). <https://doi.org/10.1016/j.jmst.2020.10.001>
12. S. Singh, A.N. Jinoop, I.A. Palani, C.P. Paul, K.P. Tomar, K.G. Prashanth, Microstructure and mechanical properties of NiTi-SS bimetallic structures built using wire arc additive manufacturing. *Mater. Lett.* **303**, 130499 (2021). <https://doi.org/10.1016/j.matlet.2021.130499>
13. S. Sridar, M.A. Klecka, W. Xiong, Interfacial characteristics of P91 steel—Inconel 740H bimetallic structure fabricated using wire-arc additive manufacturing. *J. Mater. Process. Technol.* **300**, 117396 (2022). <https://doi.org/10.1016/j.jmatprotec.2021.117396>
14. E.J. Pickering, N.G. Jones, High-entropy alloys: a critical assessment of their founding principles and future prospects. *Int. Mater. Rev.* **61**, 183–202 (2016). <https://doi.org/10.1080/09506608.2016.1180020>
15. A. Mishra, A.R. Paul, M. Mukherjee, R.K. Singh, A.K. Sharma, Evaluation of Cu-Ti dissimilar interface characteristics for wire arc additive manufacturing process. *Rapid Prototyping J.* (2022). <https://doi.org/10.1108/RPJ-05-2022-0142>
16. M. Raja, Y. Tiwari, M. Mukherjee, B. Maji, A. Chatterjee, Effect of bidirectional and switchback deposition strategies on microstructure and mechanical properties of wire arc additive manufactured Inconel 625. *Int. J. Adv. Manuf. Technol.* **119**, 4845–4861 (2022). <https://doi.org/10.1007/s00170-022-08687-2>
17. J. Baby, M. Amirthalingam, Microstructural development during wire arc additive manufacturing of copper-based components. *Weld. World.* **64**, 395–405 (2020). <https://doi.org/10.1007/S40194-019-00840-Y/FIGURES/20>
18. Y. Su, X. Hua, Y. Wu, Effect of input current modes on intermetallic layer and mechanical property of aluminum–steel lap joint obtained by gas metal arc welding. *Mater. Sci. Eng. A* **578**, 340–345 (2013). <https://doi.org/10.1016/J.MSEA.2013.04.097>
19. M. Motyka, Martensite formation and decomposition during traditional and AM processing of two-phase titanium alloys—an overview. *Metals* **11**, 481 (2021). <https://doi.org/10.3390/MET11030481>
20. P. Canale, C. Servant, Thermodynamic assessment of the Cu–Ti system taking into account the new stable phase CuTi₃. *Int. J. Mater. Res.* **93**, 273–276 (2002). <https://doi.org/10.3139/IJMR-2002-0050>
21. Y. Oshida, *Bioscience and Bioengineering of Titanium Materials*, 2nd edn. (Elsevier, Amsterdam, 2013)
22. T. Kunimine, T. Fujii, S. Onaka, N. Tsuji, M. Kato, Effects of Si addition on mechanical properties of copper severely deformed by accumulative roll-bonding. *J. Mater. Sci.* **46**, 4290–4295 (2011). <https://doi.org/10.1007/S10853-010-5235-4/FIGURES/6>
23. Y. Iguchi, G.L. Katona, C. Cserhádi, G.A. Langer, Z. Erdélyi, On the miscibility gap of Cu–Ni system. *Acta Mater.* **148**, 49–54 (2016). <https://doi.org/10.48550/1611.07068>
24. O. Taguchi, Y. Iijima, Diffusion of copper, silver and gold in α -titanium. *Philos. Mag. A* **72**, 1649–1655 (1995). <https://doi.org/10.1080/01418619508243935>
25. S.A. Chambers, D.M. Hill, F. Xu, J.H. Weaver, Silicide formation at the Ti/Si(111) interface: Diffusion parameters and behavior at elevated temperatures. *Phys. Rev. B.* **35**, 634–640 (1987). <https://doi.org/10.1103/PhysRevB.35.634>
26. A. Jain, S.P. Ong, G. Hautier, W. Chen, W.D. Richards, S. Dacek, S. Cholia, D. Gunter, D. Skinner, G. Ceder, K.A. Persson, Commentary: the materials project: a materials genome approach to accelerating materials innovation. *APL Mater.* **1**, 011002 (2013). <https://doi.org/10.1063/1.4812323>
27. A. Kale, E. Beese, T. Saenz, E. Warren, W. Nemeth, D. Young, A. Marshall, K. Florent, S.K. Kurinec, S. Agarwal, P. Stradins, Study of nickel silicide as a copper diffusion barrier in monocrystalline silicon solar cells, in *Proceedings of the 2016 IEEE 43rd*

- Photovoltaic Specialists Conference (PVSC)*, Portland, 5–10 June 2016 (IEEE, New York, 2016), pp. 2913–2916. <https://doi.org/10.1109/PVSC.2016.7750190>
28. C.S. Lee, H. Gong, R. Liu, A.T.S. Wee, C.L. Cha, A. See, L. Chan, Study of copper suicide retardation effects on copper diffusion in silicon. *J. Appl. Phys.* **90**, 3822–3824 (2001). <https://doi.org/10.1063/1.1343518>
 29. D.E. Woon, D.S. Marynick, S.K. Estreicher, Titanium and copper in Si: barriers for diffusion and interactions with hydrogen. *Phys. Rev. B.* **45**, 13383 (1992). <https://doi.org/10.1103/PhysRevB.45.13383>
 30. A. Lai, K. Bhanumurthy, G.B. Kale, B.P. Kashyap, Diffusion characteristics in the Cu–Ti system. *Int. J. Mater. Res.* **103**, 661–672 (2012). <https://doi.org/10.3139/146.110685>
 31. D. Manitsas, J. Andersson, Hot cracking mechanisms in welding metallurgy: a review of theoretical approaches. *MATEC Web Conf.* **188**, 03018 (2018). <https://doi.org/10.1051/MATECCONF/201818803018>
 32. Y. Iguchi, G.L. Katona, C. Cserháti, G.A. Langer, Z. Erdélyi, On the miscibility gap of Cu–Ni system. *Acta Mater.* **148**, 49–54 (2018). <https://doi.org/10.1016/j.actamat.2018.01.038>
 33. Y. Ustinovshikov, Phase transformations in alloys of the Ni–Cr system. *J. Alloys Compd.* **543**, 227–232 (2012). <https://doi.org/10.1016/j.jallcom.2012.05.120>
 34. Y. Kaynak, E. Tascioglu, Post-processing effects on the surface characteristics of Inconel 718 alloy fabricated by selective laser melting additive manufacturing. *Prog. Addit. Manuf.* **5**, 221–234 (2020). <https://doi.org/10.1007/s40964-019-00099-1>
 35. Y.D. Zhu, M.F. Yan, Y.X. Zhang, C.S. Zhang, First-principles investigation of structural, mechanical and electronic properties for Cu–Ti intermetallics. *Comput. Mater. Sci.* **23**, 70–78 (2016). <https://doi.org/10.1016/J.COMMATSCI.2016.06.015>

Publisher's Note Springer Nature remains neutral with regard to jurisdictional claims in published maps and institutional affiliations.

Springer Nature or its licensor (e.g. a society or other partner) holds exclusive rights to this article under a publishing agreement with the author(s) or other rightsholder(s); author self-archiving of the accepted manuscript version of this article is solely governed by the terms of such publishing agreement and applicable law.